

Stability of splay states in globally coupled rotators

Massimo Calamai,^{1,2,*} Antonio Politi,^{1,3,†} and Alessandro Torcini^{1,2,3,‡}

¹*Istituto dei Sistemi Complessi, CNR, via Madonna del Piano 10, I-50019 Sesto Fiorentino, Italy*

²*INFN Sez. Firenze, via Sansone 1, I-50019 Sesto Fiorentino, Italy*

³*Centro Interdipartimentale per lo Studio delle Dinamiche Complesse, via Sansone 1, I-50019 Sesto Fiorentino, Italy*

(Received 10 March 2009; revised manuscript received 13 August 2009; published 21 September 2009)

The stability of dynamical states characterized by a uniform firing rate (*splay states*) is analyzed in a network of N globally pulse-coupled rotators (neurons) subject to a generic velocity field. In particular, we analyze short-wavelength modes that were known to be marginally stable in the infinite N limit and show that the corresponding Floquet exponent scale as $1/N^2$. Moreover, we find that the sign, and thereby the stability, of this spectral component is determined by the sign of the average derivative of the velocity field. For leaky-integrate-and-fire neurons, an analytic expression for the whole spectrum is obtained. In the intermediate case of continuous velocity fields, the Floquet exponents scale faster than $1/N^2$ (namely, as $1/N^4$) and we even find strictly neutral directions in a wider class than the sinusoidal velocity fields considered by Watanabe and Strogatz [*Physica D* **74**, 197 (1994)].

DOI: [10.1103/PhysRevE.80.036209](https://doi.org/10.1103/PhysRevE.80.036209)

PACS number(s): 05.45.Xt, 87.19.lj, 87.10.-e

I. INTRODUCTION

Understanding the dynamical behavior of highly interconnected systems is of primary importance for neural dynamics [1], metabolic cycles [2], cold atoms [3], and synchronization in general oscillators [4]. A wide variety of interesting phenomena has been discovered, but a detailed understanding is often lacking, to the extent that even the stability properties of stationary states in globally coupled oscillators have not been fully clarified.

In this paper we study an ensemble of N identical rotators, i.e., dynamical systems characterized by a single dynamical variable, the “phase” x . This includes neural models of leaky-integrate-and-fire (LIF) type since the variable x (the membrane potential) can be interpreted as a phase. This is done by identifying the maximum value of the potential (the spiking threshold that, without loss of generality, we assume to be equal to 1) with the minimum (the resetting value assumed to be equal to 0—see the next section for further details), as if they corresponded to the angles 2π and 0. More precisely, we investigate the stability of *splay states* [5]. In a splay state all rotators follow the same periodic dynamics $x(t)$ [$x(t+T)=x(t)$] but different time shifts that are evenly distributed (and take all multiples of T/N , modulus T). Splay states have been observed experimentally in multimode laser systems [6] and electronic circuits [7]. Numerical and theoretical analyses have been performed in Josephson-junction arrays [5], globally coupled Ginzburg-Landau equations [8], globally coupled laser models [9], and pulse-coupled neuronal networks [10]. In the context of neuronal networks, splay states have been also recently investigated in systems with dynamic synapses [11] and in realistic neuronal models [12].

The first detailed stability analysis of LIF neurons was performed by developing a mean-field approach that is based

on the introduction of the probability distribution of the neuron phases [10,13]. The method is expected to work in infinite systems. More recently, another approach has been implemented [14], which is based on the linearization of a suitable Poincaré map and works for any number of oscillators. As a result, it has been discovered that the spectrum of Floquet exponents is composed of two components: (i) the growth rate of “long-wavelength” perturbations—perfectly identified also with the method described in Ref. [10]; (ii) the growth rate of “short-wavelength” (SW) perturbations that cannot be characterized with methods that involve a coarse graining over small scales. As discussed in [14], the latter component plays a crucial role when the width of the transmitted pulses is comparable to or smaller than T/N , since it may give rise to instabilities of otherwise stable patterns. The same analysis has also revealed that for finite pulse widths, SW are marginally stable in the infinite N limit. It is therefore important to investigate more thoroughly finite systems because it is still unclear whether and when they are stable.

Here we address precisely this question, by first implementing a perturbative technique in the standard LIF model and by then numerically investigating the behavior of a more general class of rotators, characterized by a nonlinear velocity field $F(x)=\dot{x}$. All of our results indicate that the SW component scales as $1/N^2$ if and only if $F(1) \neq F(0)$. Moreover, we systematically find that the SW component is stable (unstable) if $F(1) < F(0)$ [$F(1) > F(0)$]. Since $\Delta F = F(1) - F(0)$ is, by definition, the average derivative of F , the two classes of systems will be identified as decreasing and increasing fields, respectively.

At the boundary between these two classes of fields, continuous velocity fields [$F(1)=F(0)$] turn out to exhibit a faster scaling to zero of the Floquet SW spectrum. In the case of analytic functions, many exponents appear even to be numerically indistinguishable from zero. This scenario is coherent with, and in some sense extent, the theorem proved in [15], where it has been shown that in the presence of a sinusoidal field $F=a(t)+\sin(2\pi x+\alpha)$, one should expect $N-3$ zero exponents for any dependence of $a(t)$.

*massimo.calamai@gmail.com

†antonio.politi@cnr.it

‡alessandro.torcini@cnr.it

The paper is organized as follows. In Sec. II we introduce the model and the event-driven map that is used to carry out the stability analysis. In Sec. III we derive analytical perturbative expressions for the Floquet spectrum in the case of LIF neurons. The results are compared with the numerical solution of the exact equation. In Sec. IV we numerically analyze several examples of velocity fields to test the validity of the above mentioned conjectures. Finally, in Sec. V, we summarize the main results and the open problems.

II. MODEL

We consider a network of N identical neurons (rotators) coupled via a mean-field term. The dynamics of the i th neuron writes as

$$\dot{x}_i = F(x_i) + gE(t), \tag{1}$$

where x_i represents the membrane potential, $E(t)$ is the “mean” forcing field, and g is the coupling constant; the analysis will be limited to the excitatory case, i.e., $g > 0$. When the membrane potential reaches the threshold value $x_i=1$, a spike is sent to all neurons (see below for the connection between single spikes and the global forcing field E), and it is reset to $x_i=0$. The resetting procedure is an approximate way to describe the discharge mechanism operating in real neurons. The function $F(x)$ is assumed to be everywhere positive (thus ensuring that the neuron is repetitively firing, i.e., it is suprathreshold). For $F(x)=a-x$, the model reduces to the well-known case of LIF neurons. The field E is the linear superposition of the pulses emitted in the past when the membrane potential of each single neuron has reached the threshold value. By following Ref. [10], we assume that the shape of a pulse emitted at time $t=0$ is given by $E_s(t)=(\alpha^2 t/N)e^{-\alpha t}$, where $1/\alpha$ is the pulse width. This is equivalent to saying that the total field evolves according to the equation

$$\ddot{E}(t) + 2\alpha\dot{E}(t) + \alpha^2 E(t) = \frac{\alpha^2}{N} \sum_{n|t_n < t} \delta(t - t_n), \tag{2}$$

where the sum in the right-hand side (r.h.s.) represents the source term due to the spikes emitted at times $t_n < t$.

Event-driven map

As anticipated in the introduction, it is convenient to transform the differential equations into a discrete-time mapping. We do so by integrating Eq. (2) from time t_n to time t_{n+1} (where t_n is the time immediately after the n th pulse has been emitted). The resulting map reads

$$E(n+1) = E(n)e^{-\alpha\tau(n)} + Q(n)\tau(n)e^{-\alpha\tau(n)}, \tag{3a}$$

$$Q(n+1) = Q(n)e^{-\alpha\tau(n)} + \frac{\alpha^2}{N}, \tag{3b}$$

where $\tau(n)=t_{n+1}-t_n$ is the interspike time interval and, for the sake of simplicity, we have introduced the new variable $Q := \alpha E + \dot{E}$.

Moreover, the differential Eq. (1) can be formally integrated to obtain

$$x_j(n+1) = \mathcal{F}(x_j(n), E(n), Q(n), \tau(n))$$

$$j = 1, \dots, N-1; \quad x_m(n+1) \equiv 0, \tag{4}$$

where m indicates the closest-to-threshold neuron at time n and the time interval $\tau(n)$ is determined by imposing the condition that x_m reaches the value 1 at time $n+1$, immediately before being reset to zero. Altogether, we have therefore transformed the initial problem into a discrete-time map for $N+1$ variables: E , Q , and $N-1$ membrane potentials (where one degree of freedom is eliminated as a result of taking the Poincaré section). A relevant property of identical mean-field coupled rotators is that the ordering of the local variables is preserved by the dynamical evolution: all neurons “rotate” around the circle $[0,1]$ (1 being identified with 0) without passing each other. On the other hand, being the neurons identical, we can change their labels as they are indistinguishable. By following Refs. [14,16], it is convenient to start ordering the membrane potentials from the largest to the smallest one and then to introduce a co-moving reference frame, i.e., to decrease by 1 the label of each neuron (plus $1 \rightarrow N$) at each step of the iteration. In this frame, the label of the closest-to-threshold neuron is always equal to 1 and the splay state is just a fixed point of the transformation. Accordingly the linear stability analysis amounts to determining the eigenvalues of the corresponding linearized transformation.

In order to carry out the stability analysis, it is necessary to derive an explicit expression for $\mathcal{F}(x_j(n), E(n), Q(n), \tau(n))$. This is not generally doable, but in the thermodynamic limit ($N \rightarrow \infty$) one can exploit the smallness of $\tau \sim \mathcal{O}(1/N)$ and correspondingly set up a suitable perturbative expansion. We shall see that in order to correctly reproduce the stability of the splay state in typical cases, it is necessary to expand the map to fourth order. In a few peculiar models, a fully analytic calculation is possible. This is the case of LIF neurons because of the linear structure of the velocity field: they will be analyzed in the next section.

III. LEAKY INTEGRATE-AND-FIRE MODEL

Let us now consider the leaky-integrate-and-fire case for the suprathreshold neuron, namely, $a > 1$. In the co-moving frame, Eq. (4) writes as [14,16]

$$x_{j-1}(n+1) = x_j(n)e^{-\tau(n)} + 1 - x_1(n)e^{-\tau(n)} \quad j = 1, \dots, N-1, \tag{5}$$

with the boundary condition $x_N=0$, while the n th interspike interval is given by the self-consistent equation,

$$\tau(n) = \ln \left[\frac{a - x_1(n)}{a + gH(n) - 1} \right], \tag{6}$$

where

$$H(n) = \frac{e^{-\tau(n)} - e^{-\alpha\tau(n)}}{\alpha - 1} \left(E(n) + \frac{Q(n)}{\alpha - 1} \right) - \frac{\tau(n)e^{-\alpha\tau(n)}}{(\alpha - 1)} Q(n). \quad (7)$$

In the absence of coupling ($g=0$), e^τ is obviously equal to the ratio of the initial ($a-x_1$) and final ($a-1$) velocity of the first neuron, since the dynamics reduces to a pure relaxation. In that case there would be no way to determine τ as the r.h.s. would be independent of it, but with interactions this is no longer true. As soon as the coupling is switched on, the velocity starts depending on the evolution of the field E in the way that it is summarized by the expression $H(n)$.

The set of Eqs. (3a), (3b), and (5)–(7) defines a discrete-time mapping that is perfectly equivalent to the original set of ordinary differential equations. It should be noticed that Eq. (7) is valid for any physically meaningful pulse-width value (i.e., $\alpha > 0$) including $\alpha=1$, when there is no divergence or discontinuity. Moreover, in the parameter region considered in this paper (i.e., $g > 0$ and $a > 1$), the logarithm in Eq. (6) is well defined since one can show that $H(n)$ is always positive.

In this framework, the splay state reduces to a fixed point that satisfies the following conditions:

$$\tau(n) \equiv \frac{T}{N}, \quad (8a)$$

$$E(n) \equiv \tilde{E}, \quad Q(n) \equiv \tilde{Q}, \quad (8b)$$

$$\tilde{x}_{j-1} = \tilde{x}_j e^{-T/N} + 1 - \tilde{x}_1 e^{-T/N}, \quad (8c)$$

where T is the time elapsed between two consecutive spike emissions of the same neuron. A simple calculation yields

$$\tilde{Q} = \frac{\alpha^2}{N} (1 - e^{-\alpha T/N})^{-1}, \quad \tilde{E} = \tau \tilde{Q} (e^{\alpha T/N} - 1)^{-1}. \quad (9)$$

The solution of Eq. (8c) involves a geometric series that, together with the boundary condition $\tilde{x}_N=0$, leads to a transcendental equation for the period T . This, in the large N limit and at the leading order, reduces to the following simple expression:

$$\tilde{x}_j = \frac{e^T - e^{j\tau}}{e^T - 1}, \quad (10a)$$

$$T = \ln \left[\frac{aT + g}{(a-1)T + g} \right]. \quad (10b)$$

The lack of any dependence of the period from the pulse width is due to the fact that in the $N \rightarrow \infty$ limit the forcing field reduces to $\tilde{E}=1/T$ [10,14]. If we assume that $a > 1$ (which corresponds to assuming that the single neuron is suprathreshold), we see that in the excitatory case ($g > 0$) the period T is well defined only for $g < 1$ ($T \rightarrow 0$, when g approaches 1), while in the inhibitory case ($g < 0$), a meaningful solution exists for any coupling strength ($T \rightarrow \infty$ for $g \rightarrow -\infty$).

A. Linear stability

By linearizing Eqs. (3) and (5) around the fixed point (8), we obtain

$$\delta E(n+1) = e^{-\alpha\tau} \delta E(n) + \tau e^{-\alpha\tau} \delta Q(n) - (\alpha \tilde{E} - \tilde{Q} e^{-\alpha\tau}) \delta \tau(n), \quad (11a)$$

$$\delta Q(n+1) = e^{-\alpha\tau} [\delta Q(n) - \alpha \tilde{Q} \delta \tau(n)], \quad (11b)$$

$$\delta x_{j-1}(n+1) = e^{-\tau} [\delta x_j(n) - \delta x_1(n)] + e^{-\tau} (\tilde{x}_1 - \tilde{x}_j) \delta \tau(n), \quad (11c)$$

and the expression for $\delta \tau(n)$ can be derived by linearizing Eqs. (6) and (7),

$$\delta \tau(n) = \tau_x \delta x_1(n) + \tau_E \delta E(n) + \tau_Q \delta Q(n), \quad (12)$$

where $\tau_x := \partial \tau / \partial x_1$ and analogous definitions are adopted for τ_E and τ_Q .

In the co-moving frame, the boundary condition $x_N \equiv 0$ implies $\delta x_N = 0$. In practice, the stability problem is solved by computing the Floquet spectrum of multipliers $\{\mu_k\}$, $k=1, \dots, N+1$, corresponding to the linear evolution (A). It should be stressed that in general, the solution can be determined only numerically.

However, it is convenient to rewrite the Floquet multipliers as

$$\mu_k = e^{i\varphi_k} e^{T(\lambda_k + i\omega_k)/N}, \quad (13)$$

where $\varphi_k = \frac{2\pi k}{N}$, $k=1, \dots, N-1$ and $\varphi_N = \varphi_{N+1} = 0$, while λ_k and ω_k are the real and imaginary parts of the Floquet exponents. The variable φ_k plays the role of the wavenumber in the linear stability analysis of spatially extended systems and one can say that λ_k characterizes the stability of the k th mode. Previous studies [14] have shown that the spectrum can be decomposed into two components depending on the index k : (i) $k \sim \mathcal{O}(1)$; (ii) $k/N \sim \mathcal{O}(1)$. The first component corresponds to long-wavelength perturbations that can be formally analyzed by taking the continuum limit (this was implicitly done in Ref. [10]); the second component corresponds to “high” frequency oscillations that require taking in full account the discreteness of the “spatial” index j . This is clearly illustrated in Fig. 1, where we have plotted the spatial component δx_j of (the real part of) three eigenvectors. The vector plotted in panel (a) corresponds to $\varphi_k = 0.06\pi$ and is indeed both rather smooth and close to a sinusoidal function. In the other two panels, we can see that upon increasing the wavenumber φ_k , the discontinuous structure of the eigenvectors becomes increasingly evident.

While the eigenvalues of the first component are of order 1, the analysis carried out in Ref. [14] has revealed that the second component vanishes in the $N \rightarrow \infty$ limit. Therefore it is necessary to go beyond the zeroth-order result to determine the stability of a splay state in large but finite system. As an example, in Fig. 2 we show the spectrum of the Floquet multipliers of the splay state for excitatory coupling ($g > 0$) and finite values of N .

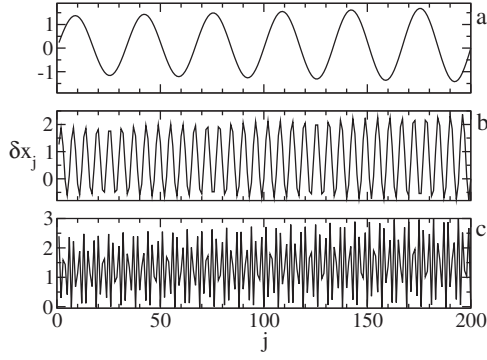


FIG. 1. Three instances of the real part of eigenvectors for LIF neurons for $a=3$, $g=0.4$, $\alpha=3$, and $N=200$. From top to bottom, panels (a)–(c) correspond to $\varphi=0.06\pi$, 0.34π , and 0.78π .

B. Analytical results

In the LIF model, many steps toward the determination of the Floquet exponents can be performed exactly. We start by deriving expressions that are valid for any number N of neurons and eventually introduce a perturbative approach to obtain an explicit expression in the large N limit.

1. Exact expressions

We start by introducing the standard Ansatz

$$\delta E(n+1) = \mu_k \delta E(n); \quad \delta Q(n+1) = \mu_k \delta Q(n). \quad (14)$$

From Eqs. (11a) and (11b)

$$\delta Q = -\frac{\alpha \tilde{Q}}{\mu_k e^{\alpha\tau} - 1} \delta\tau, \quad (15)$$

$$\delta E = -\left[\frac{\alpha\tau\tilde{Q}}{(\mu_k e^{\alpha\tau} - 1)^2} + \frac{\alpha\tilde{E} - \tilde{Q} + \alpha\tilde{Q}\tau}{\mu_k e^{\alpha\tau} - 1} \right] \delta\tau. \quad (16)$$

By combining the above equations with Eq. (12), we find

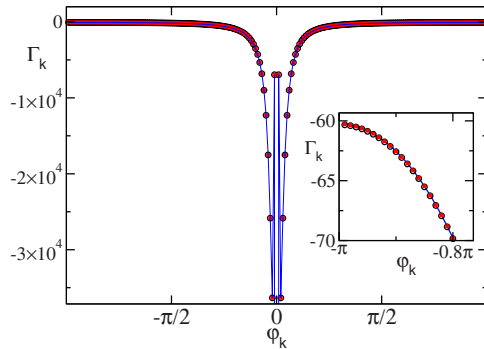


FIG. 2. (Color online) Floquet exponent spectra for the LIF neurons: exact expression (22) (filled red squares), perturbative expression (29) (blue line), and event-driven map correct up to the fourth order in τ (empty black circles). The parameters are $a=3.0$, $g=0.4$, and $\alpha=30.0$, $N=200$.

$$x_\tau = \tilde{x}_1 - a + \frac{g\tilde{Q}e^{-(\alpha-1)\tau}}{\alpha-1} + \frac{g\mu_k e^{\alpha\tau}}{(\alpha-1)(\mu_k e^{\alpha\tau} - 1)} \times \left[\alpha\tilde{E} + \frac{\tilde{Q}}{\alpha-1} + \alpha\tau\tilde{Q} \frac{(1-\mu_k e^\tau)}{(\mu_k e^{\alpha\tau} - 1)} \right], \quad (17)$$

where x_τ denotes the derivative of x_1 with respect to τ . From the evolution equation for δx_j , Eq. (11c), and by assuming that $\delta x_j(n+1) = \mu_k \delta x_j(n)$, we obtain

$$\mu_k \delta x_{j-1} = e^{-\tau} (\delta x_j - \delta x_1) + (\tilde{x}_1 - \tilde{x}_j) e^{-\tau} \delta\tau. \quad (18)$$

By using $\delta\tau = \delta x_1 / x_\tau$ and introducing the expression (8c) for \tilde{x}_j , we find

$$\mu_k \delta x_{j-1} = e^{-\tau} \delta x_j + \frac{e^{(j-1)\tau}}{e^T - 1} \frac{\delta x_1}{x_\tau} - \left(\frac{1}{x_\tau (e^T - 1)} + e^{-\tau} \right) \delta x_1. \quad (19)$$

The solution of this recursive equation reads

$$\delta x_j = -\left(\frac{1}{x_\tau (e^T - 1)} + e^{-\tau} \right) \frac{\delta x_1}{\mu_k - e^{-\tau}} + \frac{e^{j\tau}}{x_\tau (e^T - 1)} \frac{\delta x_1}{\mu_k - 1} + K \mu_k^j e^{j\tau}. \quad (20)$$

We can determine the constant K by imposing that the above equation is an identity for $j=1$. As a result,

$$\frac{\delta x_j}{\delta x_1} = \left(\frac{1}{x_\tau (e^T - 1)} + e^{-\tau} \right) \frac{\mu_k^{j-1} e^{(j-1)\tau} - 1}{\mu_k - e^{-\tau}} - \frac{e^{j\tau}}{x_\tau (e^T - 1)} \frac{\mu_k^{j-1} - 1}{\mu_k - 1} + \mu_k^{j-1} e^{(j-1)\tau}. \quad (21)$$

The equation for the determinant is finally obtained by imposing $\delta x_N = 0$,

$$x_\tau (e^T - 1) \mu_k^{N-1} = -[x_\tau (e^T - 1) + e^\tau] \frac{e^{\tau-T} - \mu_k^{N-1}}{1 - \mu_k e^\tau} + e^\tau \frac{1 - \mu_k^{N-1}}{1 - \mu_k}. \quad (22)$$

Equation (22) is an exact but implicit expression for all Floquet multipliers that applies for a generic number N of neurons. A numerical solution of Eq. (22) reveals that for finite N , excitatory coupling, and α smaller than the critical value $\alpha_c = \alpha_c(g, N)$ (see also [13]), the splay state is strictly stable, although the maximum Floquet exponent approaches zero for increasing N [14]. In fact, as shown in Ref. [14], in the limit $N \rightarrow \infty$, SW modes are marginally stable, i.e., $\lambda_k \equiv \omega_k \equiv 0$.

2. Perturbative expansion

Since the Floquet exponents of the SW vectors are exactly equal to zero in the infinite N limit, it is natural to investigate the stability of finite systems in a perturbative way. In particular, we find it convenient to introduce the smallness parameter $\tau \approx 1/N$. *A posteriori*, and in agreement with the numerical observations in [14], it turns out that an expansion up to second order in τ is necessary and sufficient to cor-

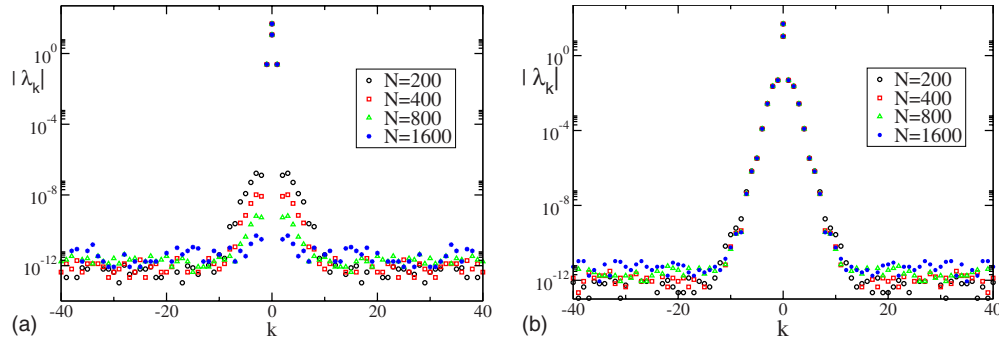


FIG. 3. (Color online) Floquet spectra: (a) single harmonic; (b) three harmonics. The parameters are $a=3.0$, $g=0.4$, and $\alpha=30.0$.

rectly determine the leading contribution of the Floquet spectrum.

Let us start by expanding the stationary solution for \tilde{Q} and \tilde{E} [Eq. (9)],

$$\tilde{Q} = \frac{\alpha}{T} \left(1 + \frac{\alpha}{2} \tau + \frac{\alpha^2}{12} \tau^2 \right), \quad (23a)$$

$$\tilde{E} = \frac{1}{T} \left(1 - \frac{\alpha^2}{12} \tau^2 \right). \quad (23b)$$

Next, we express the Floquet multipliers as

$$\mu_k = e^{i\varphi_k} e^{\Gamma_k \tau^3} \quad \mu_k^N = e^{\Gamma_k T \tau^2}, \quad (24)$$

which amounts to assume that the Floquet exponent is proportional to τ^2 .

By expanding x_τ and with the help of Eq. (10b), we obtain

$$x_\tau = - \frac{1 + \tau - B\tau^2}{e^T - 1}, \quad (25)$$

where

$$B = - \frac{1}{2} + \frac{g\alpha^2}{T} \left[\frac{1}{12} + \frac{e^{i\varphi_k}(e^T - 1)}{(e^{i\varphi_k} - 1)^2} \right]. \quad (26)$$

After inserting the above expansions into Eq. (22), we obtain

$$\begin{aligned} (-1 - \tau + B\tau^2)(\mu_k^{N-1} - \mu_k^N) &= -\tau^2 \left(B + \frac{1}{2} \right) (e^{-T} - e^{-i\varphi_k}) \\ &\quad + e^\tau (1 - \mu_k^{N-1}). \end{aligned} \quad (27)$$

Now, with the help of Eq. (24) and completing the τ expansion,

$$\Gamma_k T = \left(B + \frac{1}{2} \right) (1 - e^{-T}). \quad (28)$$

By finally replacing the definition (26) of B into the above equation, we obtain an explicit expression of the Floquet spectrum,

$$\frac{\lambda_k}{\tau^2} = \Gamma_k = \frac{g\alpha^2}{12T^2} (e^T - 2 + e^{-T}) \left[1 + \frac{6}{(\cos \varphi_k - 1)} \right]. \quad (29)$$

In Fig. 2, Eq. (29) is compared with the numerical but exact solution of Eq. (22) for $N=200$, revealing a very good agree-

ment. The divergence of this expression for $\alpha \rightarrow \infty$ indicates that the SW modes are characterized by a different scaling behavior for δ -like pulses. In fact, as shown in Ref. [14], the corresponding exponents do not scale to zero for $N \rightarrow \infty$. Moreover, it is worth recalling that the stability of networks with strictly δ pulses cannot be inferred by taking the limit $\alpha \rightarrow \infty$ of the exact (nonperturbative) expressions [14].

IV. GENERAL CASE

In the previous section we have seen that in the LIF model the SW component of the spectrum scales as $1/N^2$ and obtained an analytic expression for the leading term. It is natural to ask whether the observed scaling behavior is peculiar to this system or it is a general characteristics of pulse-coupled oscillators. For $F(x) = a + \sin(2\pi x + \alpha)$, the general theorem proved in [15] tells us that the dynamics of the oscillators is characterized precisely by $N-3$ zero exponents independently of the behavior of the forcing field E . Therefore, it is an example of perfect neutral stability for any N . For generic velocity fields, it is not possible to obtain analytic expression, so that one has to rely on approximate expressions. Since we expect $\lambda_k \rightarrow 0$ for increasing N , it is natural to follow a perturbative approach from the very beginning, i.e., from the definition of the event-driven map. In [14], it has been shown that a second-order expansion fails to reproduce the stability properties of the LIF model even on a qualitative level. In fact, the Floquet exponent of the single-step map is of order τ^3 . This would naively suggest that a third order is sufficient; however, the eigenvalue equation involves an ‘‘integration’’ over N steps. Therefore, it is necessary to control the accuracy of the single iterate of the map up to order $1/N^4$ what is incidentally guaranteed by standard integration algorithms like fourth-order Runge-Kutta. Here he have preferred to determine an explicit expression for the map to be thereby linearized and used to determine the entire Floquet spectrum. The results plotted in Fig. 2 confirm that upon including terms up to $O(1/N^4)$, we are able to reproduce the expected results.

With the goal of identifying the typical scaling behavior of the Floquet spectrum, in the following we investigate various types of functions $F(x)$, starting from smooth periodic functions. As mentioned above, if $F(x)$ contains just the main harmonic, i.e., if $F(x) = a - \sin(2\pi x)$, we expect $N-3$ zero exponents [15]. In Fig. 3(a), we plot the spectrum for $a=3$,

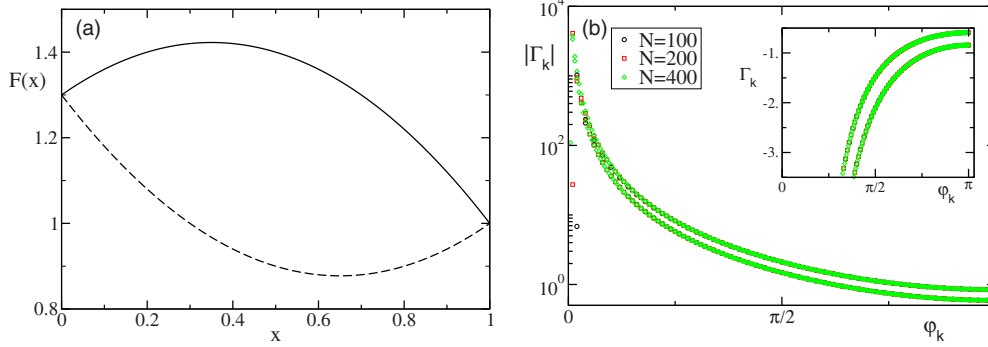


FIG. 4. (Color online) (a) The two considered velocity fields: upper and lower curves correspond to: $F(x)=1.3+0.7x-x^2$ (solid line) and $F(x)=1.3-1.3x+x^2$ (dashed line); (b) the lower (upper) Floquet spectra are associated to the lower (upper) velocity field in Fig. 4(a); please notice that in the inset due to the negative values of the spectra the correspondence is reversed. The values of the other parameters are $g=0.4$ and $\alpha=6.0$.

$g=0.4$, $\alpha=30$, and different numbers of rotators. The data indeed show that four exponents remain finite for $N \rightarrow \infty$, in agreement with the theoretical results [15], since in our system there are $N+1$ degrees of freedom. Moreover, we can see that the vast majority of the exponents are equal to zero within numerical accuracy. This is even beyond our expectations because of the finite (fourth-order) accuracy of the numerical computations.

In the presence of more harmonics, there are no theoretical predictions which can guide us. In Fig. 3(b), we present the results for $F(x)=3-\sin(2\pi x)/2-0.1\sin(4\pi x)-0.01\sin(6\pi x)$. There we see that there are no substantial differences from the previous case, the main novelty being that the number of (negative) exponents which remain finite for $N \rightarrow \infty$ is definitely larger than 4, probably 24 or 26 with our numerical accuracy. The presence of many zero exponents is confirmed by simulations performed for different parameter values. Whether the “numerical zeros” correspond to exact zeros and thereby to some conservation laws is however an open question.

The choice of a periodic function $F(x)$ such as $a-\sin(2\pi x)$ is natural in the context of coupled rotators, where x is a true phase and the 0, 1 values can be identified with one another as they correspond to angles differing by 2π . In the LIF model, 0 and 1 correspond to two different membrane potentials (actually, the minimum and maximum

accessible values) and there is no reason *a priori* to expect $F(1)=F(0)$, namely, $\Delta F=F(1)-F(0)=-1$. It is therefore important to understand whether the different scaling behavior is to be attributed to the presence of a “discontinuity” in the velocity field and if the sign of the difference $F(1)-F(0)$ matters or not. In order to clarify this point we have investigated two parabolic fields with opposite concavities, but identical (and negative) nonzero value of the velocity difference at the extrema of the definition interval, i.e., $\Delta F=-0.3$ [see Fig. 4(a) for their graphical representation]. The results plotted in Fig. 4(b) indicate that the presence of nonlinearities in the velocity field do neither affect the scaling of the spectrum, which is still proportional to τ^2 , nor the overall stability: the whole branch is strictly negative.

As a next step, we have investigated two increasing parabolic velocity fields with opposite concavities, but identical and positive difference at the extrema $\Delta F=0.3$ [see Fig. 5(a) for a graphical representation]. The results plotted in Fig. 5(b) confirm once again the τ^2 scaling. However, the stability has changed: now the SW component is positive, indicating that the splay state is weakly unstable. Altogether, we can summarize the results under the conjecture that all discontinuous velocity fields [i.e., where $F(1) \neq F(0)$] are characterized by exponents that scale as τ^2 . Moreover, the stability depends on whether on the average the field increases or decreases. The analysis of several other velocity fields has confirmed this conjecture.

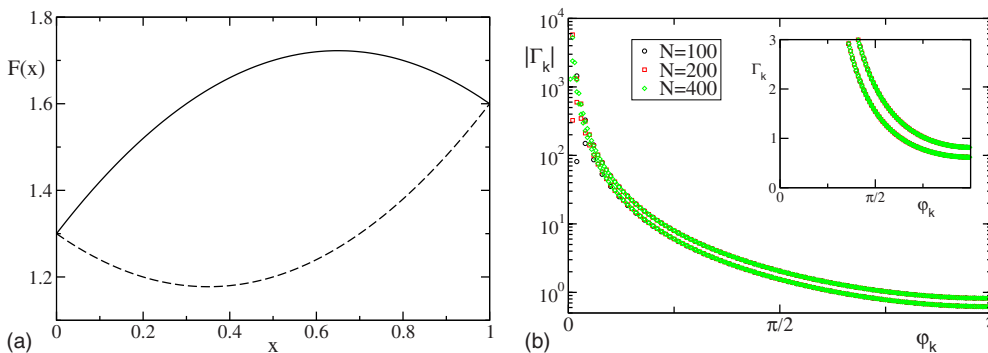


FIG. 5. (Color online) (a) The two considered velocity fields: upper and lower curves correspond to: $F(x)=1.3+1.3x-x^2$ and $F(x)=1.3-0.7x+x^2$; (b) the lower (upper) Floquet spectra are associated to the lower (upper) velocity field in Fig. 5(a). The values of the other parameters are $g=0.4$ and $\alpha=6.0$.

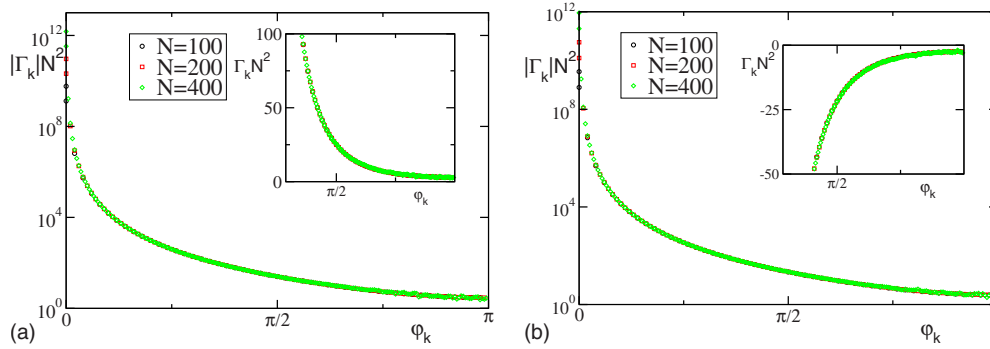


FIG. 6. (Color online) Floquet spectra: (a) continuous parabolic field $F(x)=1.3-x(x-1)$; (b) continuous sinusoidal field $F(x)=1.3-0.25 \sin(\pi x)$ with period 2. The data refer to $g=0.4$ and $\alpha=6$ and have been obtained by employing an event-driven map including terms up to order $\mathcal{O}(1/N^5)$.

In between the two classes of increasing and decreasing fields, there are continuous fields. The neutral stability of the sinusoidal fields is logically consistent with the observation that the stability depends on the sign of ΔF . In order to further explore the generality of the scenario, we have analyzed two other cases: (i) a parabolic field $F(x)=1.3-x(x-1)$; (ii) a sinusoidal field $F(x)=1.3-0.25 \sin(\pi x)$. Both fields are C^0 , but not C^1 , since the derivative in $x=1$ and $x=0$ differ from one another. In Fig. 6 we see that the spectra scale as $1/N^4$. This confirms that continuous functions exhibit an intermediate behavior between positive and negative discontinuities. The scaling behavior, as τ^4 , has been verified by employing an event-driven map correct to order τ^5 . Moreover, it is also interesting to notice the difference with respect to the analytic sinusoidal functions. In fact, it seems that exactly zero exponents are detected only for analytic velocity fields.

To further verify the scenario, we have introduced a velocity field

$$F(w) = a + 4w(w-1),$$

$$w = (x^\gamma + x)/2, \quad (30)$$

parametrized by the exponent γ . The function is periodic but, upon increasing γ , it becomes increasingly steeper in the vicinity of $x=1$ as shown in Fig. 7(a). For $\gamma < 10$ we observe the same behavior found for other periodic functions, i.e., the spectrum scales rapidly to zero (like $1/N^4$). To exemplify this case let us consider $\gamma=2$, as shown in Fig. 7(b) the eigenvalue $\Gamma_{N/2}$ decreases as $\sim 1/N^2$ for sufficiently large N . Please notice that the eigenvalues are approaching zero from positive values in this case. For $\gamma \sim 10^2$ the situation becomes more complicated: for sufficiently small N values $\Gamma_{N/2}$ is negative and almost constant (indicating a $1/N^2$ scaling of the Floquet eigenvalues), while by increasing N it becomes positive and $\Gamma_{N/2} \rightarrow 0$ only for very large N , $\Gamma_{N/2} \rightarrow 0$ [see Fig. 7(c)]. By increasing γ , the $1/N^2$ scaling region widens, but the overall behavior is maintained, as shown in Fig. 7(d) for $\gamma=10\,000$. This suggests that for not too large values of N , the system perceives the field as if it was discontinuous, while at large N it crosses to continuous fields. This crossing is joined to a change in sign from nega-

tive values (as expected for discontinuous fields with $\Delta F < 0$) to positive ones.

Finally, for the sake of mathematical generality, we have investigated the role of an additional intermediate discontinuity in the velocity field. More precisely, we have examined the piecewise linear model,

$$F(x) = \begin{cases} a - b/2 - x, & \text{for } x \leq 0.5 \\ a + b/2 - x, & \text{for } x > 0.5, \end{cases} \quad (31)$$

with a discontinuity of size b at $x=0.5$. As shown in Fig. 8(a), as a result of the discontinuity, the Floquet spectrum widens to cover a thick band, which is filled in an increasingly uniform way, upon increasing N . Depending whether the discontinuity is positive or negative, the band develops toward higher or smaller values, respectively [see Fig. 8(b)], while the standard LIF spectrum (solid line) represents the locus of minima or maxima, respectively, of such bands. Due to the finite thickness of the band itself, unstable SW modes can appear even for $\Delta F < 0$. Finally, for $b=1$, when $\Delta F = F(1) - F(0) = 0$, the SW modes scale faster than $1/N^2$ as for standard continuous functions. Altogether, the presence of an additional discontinuity does not modify the scaling behavior, which is still controlled by the sign of ΔF .

V. CONCLUSIONS AND OPEN PROBLEMS

In this paper we have shown that the stability of splay states in pulse-coupled oscillators with generic velocity fields $F(x)$ can be determined by rewriting the dynamics as event-driven maps. In particular we focused our attention on the SW modes. For discontinuous velocity fields, like that associated to leaky-integrate-and-fire neurons, we find that all SW modes are stable, when the field on the average decreases (i.e., $\Delta F < 0$), and unstable in the opposite case. Notice that this weak instability cannot be captured by the mean-field approach introduced in [10], as the coarse graining washes out SW modes. It is instructive to compare the role of ΔF , with the results of Refs. [17,18]. While studying an excitatory network of globally coupled rotators (in the limit of δ -like pulses), Mirollo and Strogatz proved that the synchronous state is fully stable when $x(\phi)$ is concave-down [17], where the phase ϕ is nothing but the time variable

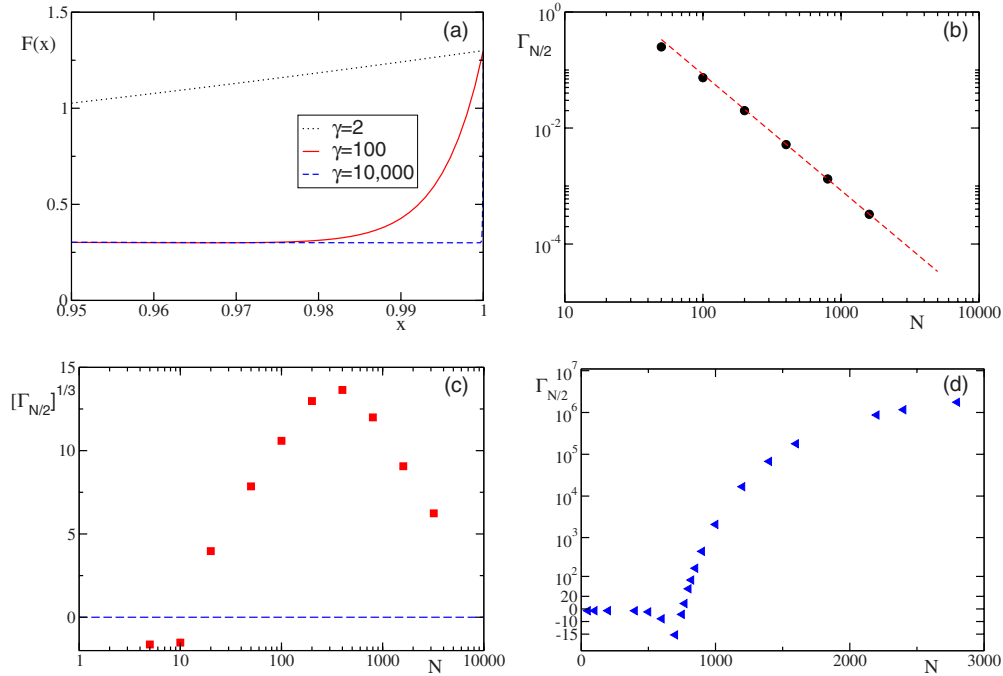


FIG. 7. (Color online) (a) The velocity fields expressed by Eqs. (30) for three different γ values are reported in proximity of $x=1$. The stability exponent $\Gamma_{N/2}$ corresponding to the highest frequency ($\varphi_{N/2}=\pi$) is plotted in panels (b), (c), and (d) for the three different γ values as a function of N . In (b), the (black) filled circles refer to $\gamma=2$ and the dashed (red) line represents a power-law decay $N^{-\beta}$ with $\beta=2$. In (c), $[\Gamma_{N/2}]^{1/3}$ is displayed for $\gamma=100$; the dashed (blue) line indicates the zero axis. Finally, for a better visualization of the data for $\gamma=10\,000$, the vertical scale in (d) has been obtained by first shifting $\Gamma_{N/2}$ by 20 units and thereby using exponentially separated units. All eigenvalues refer to $a=1.3$, $g=0.4$, and $\alpha=6$.

(apart from a scaling factor) and the evolution refers to the single neuron dynamics $\dot{x}=F(x)$. Recently, these results have been complemented by the observation that clustered states are stable (while the synchronous regime is unstable), when $x(\phi)$ is concave-up [18–20]. It is easy to verify that in a linear LIF neuron, the change in concavity is one-to-one connected with a change in sign of ΔF . More in general, a concave-up (-down) $x(t)$ implies that $\Delta F > 0$ ($\Delta F < 0$), while the opposite implication does not hold. For instance, for $F(x)=1.3-\sin[\pi(9x-1)/4]$ ($x \in [0,1]$), $x(t)$ exhibits even two changes of concavity and yet we find that the SW modes are stable and scale as $1/N^2$, as expected, since $\Delta F=-\sqrt{2}/2$. Altogether, the condition arising from the sign of F is more

general than that based on the sign of the concavity of $x(t)$, but it refers to SW modes only.

Naively, one might think that our results follow from the fact that ΔF is the average derivative of the velocity field in the interval $[0,1]$. If, on the average, $\dot{x}=(\Delta F)x$, it is natural to expect exponential instability when $\Delta F > 0$, stability in the opposite case, and marginal stability for $\Delta F=0$. However, to leading order, all SW modes are “marginally” stable. Presumably, there is some truth in the argument, but some refinements are required to put it on a firm basis. Furthermore, the $1/N^2$ scaling of the Floquet spectrum has been so far rigorously proved for LIF neurons and has been confirmed by the numerical analysis of several nonlinear fields. This

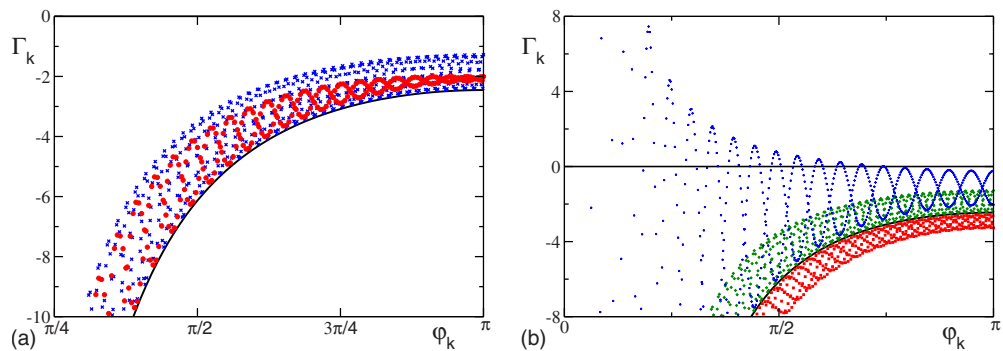


FIG. 8. (Color online) Floquet spectra Γ_k associated to the velocity field (31). (a) Spectra for various N with $b=+0.2$: $N=800$ (red) circles and $N=1600$ (blue) crosses. (b) Spectra for $N=1600$ at different b values: namely, (red) squares refer to $b=-0.2$, (green) diamonds to $b=+0.2$, and (blue) stars to $b=+0.6$. For comparison also the Floquet spectrum corresponding to a LIF neuron with the same parameters is reported (black solid line). All the data refer to $a=1.7$, $g=0.4$, and $\alpha=6$.

includes the well-known exponential integrate-and-fire neurons [21]—which, having a discontinuous velocity field with $\Delta F < 0$, are consistently characterized by stable SW modes.

The intermediate case of continuous velocity fields presents even more subtleties. They are generically characterized by a $1/N^4$ scaling to zero, but we are unable to conclude whether the scaling law is entirely determined by the analyticity properties of the velocity field. Anyway, for fields composed of a few harmonics, it appears that all Floquet exponents (with the exception of a finite number of them) are equal to zero. These results suggest that perfectly marginal modes exist in a wide range of cases than those proved in [15] and shown in [22]. The question is not of purely academic interest since analytic velocity fields are generically encountered when dealing with coupled rotators, where

x is a true phase. Furthermore, the so-called quadratic integrate-and-fire neurons [23] belong to this class, as the velocity field is $F(x) = dx(1-x) + e$ and it is therefore continuous. We have verified that this model is not an exception, as its short-wavelength spectrum scales faster than $1/N^2$.

ACKNOWLEDGMENTS

We acknowledge useful discussions with F. Ginelli, M. Timme, M. Wolfrum, and S. Yanchuk, as well as a constructive interaction with S. Strogatz. This work has been partly carried out with the support of the EU under Project No. NEST-PATH-043309 and of the Italian project “Struttura e dinamica di reti complesse” N. 3001 within the CNR program “Ricerca spontanea a tema libero.”

-
- [1] D. J. Amit, *Modeling Brain Function: The World of Attractor Neural Networks* (Cambridge University Press, New York, 1990).
- [2] D. Fell, *Understanding the Control of Metabolism* (Portland Press, London, 1997).
- [3] J. Javaloyes, M. Perrin, and A. Politi, Phys. Rev. E **78**, 011108 (2008).
- [4] Y. Kuramoto, *Chemical Oscillations, Waves, and Turbulence* (Springer-Verlag, Berlin, 1984).
- [5] S. Nichols and K. Wiesenfeld, Phys. Rev. A **45**, 8430 (1992); S. H. Strogatz and R. E. Mirollo, Phys. Rev. E **47**, 220 (1993).
- [6] K. Wiesenfeld, C. Bracikowski, G. James, and R. Roy, Phys. Rev. Lett. **65**, 1749 (1990).
- [7] P. Ashwin, G. P. King, and J. W. Swift, Nonlinearity **3**, 585 (1990).
- [8] V. Hakim and W.-J. Rappel, Phys. Rev. A **46**, R7347 (1992).
- [9] W.-J. Rappel, Phys. Rev. E **49**, 2750 (1994).
- [10] L. F. Abbott and C. van Vreeswijk, Phys. Rev. E **48**, 1483 (1993).
- [11] P. C. Bressloff, Phys. Rev. E **60**, 2160 (1999).
- [12] N. Brunel and D. Hansel, Neural Comput. **18**, 1066 (2006).
- [13] C. van Vreeswijk, Phys. Rev. E **54**, 5522 (1996).
- [14] R. Zillmer, R. Livi, A. Politi, and A. Torcini, Phys. Rev. E **76**, 046102 (2007).
- [15] S. Watanabe and S. H. Strogatz, Physica D **74**, 197 (1994).
- [16] R. Zillmer, R. Livi, A. Politi, and A. Torcini, Phys. Rev. E **74**, 036203 (2006).
- [17] R. E. Mirollo and S. H. Strogatz, SIAM J. Appl. Math. **50**, 1645 (1990).
- [18] A. Mauroy and R. Sepulchre, Chaos **18**, 037122 (2008).
- [19] In a quite recent work Kirst *et al.* [20] have shown for a simple model of spiking neuron, with a concave-up $x(\phi)$ and with a *partial reset*, that synchronous and clustered state can coexist. This finding somehow contradicts the results reported in [17,18].
- [20] C. Kirst, T. Geisel, and M. Timme, Phys. Rev. Lett. **102**, 068101 (2009).
- [21] N. Forcaud-Trocmé, D. Hansel, C. van Vreeswijk, and N. Brunel, J. Neurosci. **23**, 11628 (2003).
- [22] D. Golomb, D. Hansel, B. Shraiman, and H. Sompolinsky, Phys. Rev. A **45**, 3516 (1992).
- [23] W. Gerstner and W. M. Kistler, *Spiking Neuron Models: Single Neurons, Populations, Plasticity* (Cambridge University Press, Cambridge, 2002).